Experimental Gerontology 224 (2026) 113318

Contents lists available at ScienceDirect

Experimental Gerontology

journal homepage: www.elsevier.com/locate/expgero

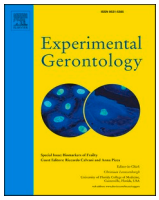

Epigenetic aging and autosomal methylation remodeling in Anderson-Fabry disease☆

Mirella Aurora Aceto [a], Ersilia Paparazzo [a], Gemma Antonucci [a], Rosita Greco [b], Michele Andreucci [c], Teresa Serra Cassano [a,d], Pierluigi Mercatante [a,d], Giuseppe Passarino [a,1], Antonella La Russa [c], Alberto Montesanto [a,*,2]

[a] Department of Biology, Ecology and Earth Sciences, University of Calabria, 87036, Rende, Italy
[b] Nephrology, Dialysis and Renal Transplant Unit, Hospital 'SS. Annunziata', Cosenza, Italy
[c] Department of Medical and Surgical Sciences, Magna Graecia University of Catanzaro, Catanzaro, Italy
[d] University of Florence, Department of Statistic, Computer Science and Application, DiSIA, Viale Morgagni, 59, Florence, FI 50134, Italy

ARTICLE INFO

Section editor: Christiaan Leeuwenburgh

Keywords:
Anderson-Fabry disease
DNA methylation
Epigenetic aging
Epigenome-wide association study
Lysosomal storage disorders
Epigenetic clock

ABSTRACT

Anderson-Fabry disease (AFD) is a rare X-linked lysosomal storage disorder characterized by marked clinical heterogeneity and incompletely understood genotype-phenotype correlations. While X-chromosome inactivation has been extensively investigated, the contribution of autosomal epigenetic mechanisms to phenotypic variability remains poorly defined. Here, we performed an exploratory genome-wide DNA methylation analysis in 32 AFD patients (22 females and 10 males; mean age 51.7 years) recruited within a multicenter regional research project in Calabria (Italy). DNA methylation profiling was conducted using the Infinium MethylationEPIC v2.0 array. The analysis integrated two complementary approaches: differential methylation analysis and evaluation of biological aging through multiple epigenetic clocks, including Horvath, Hannum, PhenoAge, Skin & Blood, GrimAge, and DunedinPACE.

Exploratory methylome-wide analysis identified a limited set of CpG loci showing nominal evidence of methylation differences between carriers of pathogenic and non-pathogenic variants; however, none remained statistically significant after correction for multiple testing. Annotation of the top-ranking nominal CpG associations highlighted genes involved in biological processes including vascular regulation, intracellular trafficking, cytoskeletal organization, immune signaling, and lipid metabolism. No significant differences between groups were observed for the conventional epigenetic age-acceleration measures examined. In contrast, carriers of pathogenic variants showed significantly higher DunedinPACE values ($p = 0.0328$), indicating a faster estimated pace of biological aging. This finding suggests that DunedinPACE may capture aspects of the cumulative systemic burden associated with pathogenic GLA variants, although confirmation in larger independent cohorts is required.

Overall, this pilot epigenomic study provides preliminary evidence that autosomal epigenetic remodeling and biological aging acceleration may contribute to phenotypic heterogeneity in AFD.

1. Introduction

Anderson-Fabry disease (AFD) is a rare X-linked lysosomal storage disorder caused by pathogenic variants in the *GLA* gene, located on Xq22, which encodes the enzyme α-galactosidase A (α-Gal A) (Germain et al., 2022). This enzyme catalyses the intracellular hydrolysis of terminal non-reducing alpha-D-galactose residues in alpha-D-galactosides, including galactooligosaccharides, galactomannans and galactolipids

☆ This article is part of a Special issue entitled: 'Molecular and Epigenetic Aspects of Aging' published in Experimental Gerontology.

* Corresponding author at: Department of Biology, Ecology and Earth Sciences, University of Calabria, 87036, Rende, CS, Italy.
E-mail address: alberto.montesanto@unical.it (A. Montesanto).

[1] Given his role as Executive Guest Editor, Giuseppe Passarino had no involvement in the peer-review of this article and has no access to information regarding its peer-review. Full responsibility for the editorial process for this article was delegated to another journal editor.

[2] Present address.

https://doi.org/10.1016/j.exger.2026.113318
Received 21 May 2026; Received in revised form 2 September 2026; Accepted 8 September 2026
Available online 9 September 2026

(Schiffmann, 2024). Mutations in *GLA* lead to reduced or absent α-Gal A activity, resulting in progressive accumulation of globotriaosylceramide (Gb3) and other glycosphingolipids within lysosomes, ultimately affecting multiple organ systems, including the kidneys, heart, and nervous system (Zarate and Hopkin, 2008). The initial pathological event is the accumulation of Gb3 in various cell types, including endothelial cells, neurons, cardiomyocytes, and cells of the reticuloendothelial system, which triggers cellular dysfunction and activates pathogenic pathways responsible for progressive multi-organ damage. Being a multisystemic disorder, AFD affects several organs, with pathogenic mechanisms varying depending on the type of cell or tissue involved (Tuttolomondo et al., 2013). Clinically, AFD presents with heterogeneous features that depend on gender, genotype, and the severity of the enzymatic defect. Two main clinical phenotypes are identified: a classic and a non-classic or late-onset phenotype. The classic form, predominantly affecting males, is characterized by absent or markedly reduced (<3% of normal) α-Gal A activity, leading to early childhood symptoms such as acroparesthesias, angiokeratomas, cornea verticillata, gastrointestinal complaints, and hypohidrosis (Germain et al., 2022). As the disease progresses, renal, cardiac, and cerebrovascular complications develop, often manifesting between the second and fourth decades of life. In contrast, individuals with late-onset AFD exhibit residual enzyme activity and a more restricted clinical profile, typically presenting with cardiac involvement in adulthood, while other classic manifestations may be absent or mild (Pieroni et al., 2024).

To date, 1179 mutations in the *GLA* gene have been identified, with missense mutations being the most prevalent, alongside nonsense mutations, insertions, deletions, and splicing alterations [The Human Gene Mutation Database. 2021. Available online: http://www.hgmd.cf.ac.uk/ac/gene.php?gene=GLA (accessed on May 7th, 2025)]. Mutations causing complete loss of enzyme function are typically associated with the classic, severe phenotype, while missense mutations leading to residual enzyme activity may manifest as milder, later-onset forms (Simonetta et al., 2018). Most patients harbor "private variants", mutations unique to their family, yet significant intrafamilial phenotypic variability is frequently observed (Schiffmann, 2024; Simonetta et al., 2018). In addition, despite having the same pathogenic mutation, phenotypes may vary widely also within different families making genotype-phenotype determination very difficult (Viggiano and Politano, 2021). Thus, AFD is characterized by phenotypic heterogeneity which is inter- and intrafamilial (Tuttolomondo et al., 2017). Consequently, establishing genotype–phenotype correlations has proven challenging, as other factors such as genetic background, epigenetic modifications, and environmental influences likely contribute to disease expression and progression. Importantly, in female patients, an additional layer of phenotypic heterogeneity arises due to X-chromosome inactivation (XCI) (Balaton et al., 2018; Furlan and Galupa, 2023). In fact, although traditionally considered asymptomatic carriers, many heterozygous females manifest clinical signs of AFD, sometimes as severe as in males. This variability is largely attributed to the pattern of XCI: when the X chromosome carrying the normal GLA allele is preferentially inactivated (skewed XCI), more cells express the mutant allele, leading to reduced overall α-Gal A activity and more severe phenotypes. Conversely, if the X chromosome with the mutant allele is preferentially inactivated, females may exhibit milder or no symptoms (Viggiano and Politano, 2021).

Thus, given its crucial role in shaping phenotypic variability among female heterozygotes, both XCI and DNA methylation focused on the X chromosome have been extensively studied in the context of AFD (Wagenhäuser et al., 2022; Ŕeboun et al., 2022; De Riso et al., 2020; Di Risi et al., 2021; Iza et al., 2025). In contrast, the potential role of epigenetic mechanisms related to autosomal (non-sex) chromosomes in modulating phenotypic variability in AFD has not yet been widely investigated (Di Risi et al., 2022). Among emerging epigenetic tools, epigenetic clocks, which estimate biological age based on DNA methylation patterns, have shown promise in various disease contexts as biomarkers of systemic stress, cellular aging, and chronic inflammation. Applying these clocks to AFD patients may help explain part of the observed clinical heterogeneity, particularly in those cases where chronological age does not align with disease severity or with its progression (Freire-Aradas et al., 2020; Garali et al., 2020).

Given the current lack of data on epigenetic aging in AFD, our study aimed to explore genome-wide autosomal DNA methylation patterns and biological aging within a clinically ascertained cohort of individuals with AFD. Participants were stratified according to the ClinVar classification of their GLA variants into carriers of pathogenic and non-pathogenic variants, with the latter group including several variants classified as variants of uncertain significance (VUS). This within-cohort comparison was selected as an exploratory approach to investigate whether the presence of a GLA variant with established pathogenic significance was associated with differences in autosomal DNA methylation patterns and biological aging measures. Importantly, since the comparison was not performed against a healthy control group, the present study was aimed at identifying preliminary epigenetic differences associated with GLA variant classification within the study cohort. To this end, we integrated two complementary approaches: (i) exploratory differential methylation analysis at individual CpG sites and (ii) assessment of biological aging using established epigenetic clocks.

2. Materials and methods

2.1. Participant characteristics

For this study, 32 individuals diagnosed with AFD were enrolled (mean age, 51.69 years; 22 females and 10 males).

Patients were recruited from two operative units (Nephrology Unit of the Azienda Ospedaliera of Cosenza, Italy, and the Nephrology Unit of the Azienda Ospedaliero-Universitaria "Renato Dulbecco" of Catanzaro, Italy) participating in an ongoing regional multicenter research project carried out in Calabria (Italy) starting from 2024. The diagnosis of AFD was established based on clinical evaluation, confirmed through molecular genetic sequencing identifying variants in the GLA gene, and supported by biochemical testing of α-galactosidase A enzyme activity. Among the enrolled subjects, 26 had variants associated with late-onset AFD and 6 with early-onset AFD; among enrolled subjects, 24 carried variants of uncertain significance (VUS), whereas 8 carried pathogenic variants. These variants have been classified according to the ClinVar database. At the time of enrolment, 6 participants were already receiving enzyme replacement therapy (ERT) with agalsidase, whereas 26 were untreated. Patient genetic and clinical characteristics, including α-Gal A level of activity, are shown in Table 1.

For the subsequent analyses, participants were stratified according to the ClinVar classification of their GLA variants into carriers of pathogenic and non-pathogenic variants. The non-pathogenic group included several variants classified as variants of uncertain significance (VUS) and was not intended to represent a healthy or unaffected control group.

2.2. Blood collection and DNA extraction

Peripheral blood samples were collected in tubes containing EDTA and stored frozen at −20 °C. Genomic DNA was extracted using the Invitrogen™ PureLink™ Genomic DNA Mini Kit. Extracted DNA was quantified using a NanoDrop™ One (Thermofisher). Written informed consent was obtained from all participants, and all the studies were approved by the Regional Ethical Committee, Catanzaro, Italy (Prot. CET 200/2024).

2.3. Infinium HumanMethylation EPICv2 BeadChip array

Microarray hybridization was performed by Genomix4Life srl (Baronissi, SA, Italy). DNA samples from the cohort used to develop the aforementioned model were processed following standard procedures.

Table 1
Genetics and clinical characteristics of the study cohort. M = male, F = female; SNV = Single Nucleotide Variant; VUS = variant of unclear significance.

Sample	Age	Sex	Gene Variant	Onset	Type and Classification of Variant	Interpretation of Variant (ClinVar-NCBI)	α-gal A Activity	Clinical Involvement	Therapy
FD1	64	F	p.N5D	Late	SNV missense	Pathogenic	>15 nmol/ml/h	Renal	NO
FD2	68	M	p.D313Y	Late	SNV missense	VUS	>15 nmol/ml/h	Neurological	NO
FD3	44	M	p.N53Nfs*68	Early	Frameshift	Pathogenic	<0.3 nmol/ml/h	Renal, Cardiac	YES
FD4	45	F	IVS5 + 1G > T	Early	Intronic	Pathogenic	4.7 nmol/ml/h	Renal, Cardiac	NO
FD5	30	F	p.D313Y	Late	SNV missense	VUS	>15 nmol/ml/h	–	NO
FD6	20	F	p.D313Y	Late	SNV missense	VUS	>15 nmol/ml/h	–	NO
FD7	63	F	p.D313Y	Late	SNV missense	VUS	>15 nmol/ml/h	Neurological	NO
FD8	44	M	p.D313Y	Late	SNV missense	VUS	>15 nmol/ml/h	Neurological	NO
FD9	78	F	p.N53Nfs*68	Early	Frameshift	Pathogenic	3.2 nmol/ml/h	Renal	YES
FD10	64	F	p.D313Y	Late	SNV missense	VUS	>15 nmol/ml/h	Neurological	NO
FD11	59	F	p.D313Y	Late	SNV missense	VUS	>15 nmol/ml/h	Renal, Cardiac	NO
FD12	35	F	p.D313Y	Late	SNV missense	VUS	>15 nmol/ml/h	Neurological	NO
FD13	65	M	p.D313Y	Late	SNV missense	VUS	7 nmol/ml/h	Renal, Cardiac	NO
FD14	64	F	p.D313Y	Late	SNV missense	VUS	>15 nmol/ml/h	Neurological	NO
FD15	29	F	p.D313Y	Late	SNV missense	VUS	>15 nmol/ml/h	Cardiac	NO
FD16	80	F	p.D313Y	Late	SNV missense	VUS	>15 nmol/ml/h	Neurological	NO
FD17	59	M	p.D313Y	Late	SNV missense	VUS	>15 nmol/ml/h	Neurological	NO
FD18	56	F	c.370-2 A > G	Early	Splice site	Pathogenic	>15 nmol/ml/h	Renal, Neurological	YES
FD19	69	F	p.S126G	Late	SNV missense	VUS	14.4 nmol/ml/h	Renal	YES
FD20	65	F	p.D313Y	Late	SNV missense	VUS	>15 nmol/ml/h	Renal	YES
FD21	46	M	p.D313Y	Late	SNV missense	VUS	>15 nmol/ml/h	–	NO
FD22	47	F	p.D313Y	Late	SNV missense	VUS	>15 nmol/ml/h	Neurological	NO
FD23	21	F	p.D313Y	Late	SNV missense	VUS	>15 nmol/ml/h	–	NO
FD24	62	F	p.D313Y	Late	SNV missense	VUS	>15 nmol/ml/h	Neurological	NO
FD25	19	M	p.D313Y	Late	SNV missense	VUS	>15 nmol/ml/h	Renal, Neurological	NO
FD26	42	F	p.S126G	Late	SNV missense	VUS	>15 nmol/ml/h	Renal	NO
FD27	50	F	p.D313Y	Late	SNV missense	VUS	>15 nmol/ml/h	Renal, Neurological	NO
FD28	57	F	p.D313Y	Late	SNV missense	VUS	>15 nmol/ml/h	Neurological	NO
FD29	50	M	p.N215S	Late	SNV missense	Pathogenic	7 nmol/ml/h	Renal	NO
FD30	48	M	c.999 + 1G > T	Early	Splice site	Pathogenic	0.2 nmol/ml/h	Renal	NO
FD31	49	M	p.Q283DfsTer15	Early	Frameshift	Pathogenic	<0.3 nmol/ml/h	Renal, Cardiac	YES
FD32	59	F	p.D313Y	Late	SNV missense	VUS	>15 nmol/ml/h	Renal, Neurological	NO

Briefly, 8.9 ng of genomic DNA was quantified using a NanoDrop™ One spectrophotometer (Thermo Fisher Scientific) and subsequently subjected to bisulfite conversion using the EZ DNA Methylation Kit (Zymo Research, Irvine, CA, USA), according to the manufacturer's instructions. The converted DNA was then processed following Illumina protocols and hybridized onto the Infinium MethylationEPIC v2.0 BeadChip (Illumina Inc., CA, USA). All 32 samples were processed simultaneously to minimize batch effects.

2.4. Bioinformatics and statistical analysis

2.4.1. Quality control/data-processing

DNA methylation data were analysed in the R environment using the MeCallR pipeline (Yang and Han, 2024), following a standardized and reproducible workflow. Raw intensity files were first imported and subjected to systematic quality control at both the sample and probe levels. Sample quality assessment was conducted using the *minfi* package. A predefined exclusion threshold of 10.5 was applied in order to ensure high data reliability. Samples not meeting this quality criterion were excluded from downstream analyses. Probe-level filtering was

performed using the MeCall.Filtering function. Several categories of probes were removed to minimize technical bias and avoid spurious biological signals. Specifically, probes with detection *P*-values >0.01 were excluded to ensure measurement reliability. Probes with an insufficient beadcount were removed to avoid instability in methylation estimates. Probes located in non-CpG regions were excluded, as were probes known to overlap single-nucleotide polymorphisms (SNPs), which may affect hybridization specificity. Multi-hit probes mapping to multiple genomic loci were also removed to prevent ambiguous signal attribution. In addition, probes located on sex chromosomes were excluded to avoid sex-driven methylation differences that could confound group comparisons. Probes flagged for known reliability issues, probes not correctly mapped to the GRCh38/hg38 reference genome, and duplicate probes present in the EPICv2 platform were also discarded. Following filtering, data normalization was performed using the MeCall.Norm function. Background correction was applied using the Noob method, and beta values were normalized using BMIQ to correct for probe-type bias. Outlier detection was subsequently performed using the MeCall.Outlier function. Finally, potential batch effects were assessed using MeCall.FindBatch, in order to identify any technical variation that might require correction before differential methylation analyses.

2.4.2. Cell type correction

To reduce potential *bias* due to differences in blood cellular composition, the proportions of the main leukocyte populations were estimated using a deconvolution approach based on whole blood reference data, implemented in the *minfi* package. Specifically, the proportions of CD4 and CD8 T lymphocytes, NK cells, B cells, monocytes, and neutrophils were obtained (Aryee et al., 2014; Houseman et al., 2012). To formally assess differences in leukocyte composition between carriers of pathogenic and non-pathogenic GLA variants, estimated cell proportions were compared using Welch's two-sample *t*-test. Mean differences and corresponding 95% confidence intervals were calculated, and *P*-values were adjusted for multiple testing across the six leukocyte populations using the Benjamini–Hochberg false discovery rate (FDR) method.

2.4.3. Epigenetic aging calculation

Age acceleration estimates were derived from the residuals of linear regression models of DNA methylation (DNAm) age on chronological age using the methylclock package. Specifically, the main epigenetic clocks, Horvath (Horvath, 2013), SkinBlood-Horvath (Horvath et al., 2018), Levine (Levine et al., 2018), Hannum (Hannum et al., 2013), EN (Robinson, 1991), and BLUP (Zou and Hastie, 2005), were computed, and for each clock, the age acceleration was defined as the residuals obtained by regressing DNAm age on chronological age (Pelegí-Sisó et al., 2021; Teschendorff and Horvath, 2025). In addition, the DunedinPACE score was calculated to estimate the pace of biological aging (Belsky et al., 2022). DunedinPACE was additionally included as a complementary aging measure because, unlike conventional epigenetic clocks that estimate biological age, it was specifically developed to quantify the pace of biological aging. Therefore, its inclusion allowed us to assess whether GLA variant classification was associated not only with deviations between DNAm-predicted and chronological age but also with differences in the estimated rate of biological aging.

2.4.4. Differentially methylated position analysis

To identify mean methylation differences between pathogenic and non-pathogenic AFD patients, we performed differential methylation analyses at the single-site (DMP) level using the R package *limma (*Peters et al., *2015)*. DMPs were identified by comparing M-values at each cytosine CpG locus between patients with pathogenic AFD and patients with non-pathogenic AFD. *P*-values were adjusted for multiple testing using the Benjamini–Hochberg false discovery rate (FDR) method. All analyses were conducted on M-values, derived from β-values to better satisfy the assumptions of linear modeling (Du et al., 2010). Models were also adjusted for potential confounders, including age, sex, treatment, and estimated leukocyte composition. Experimental slide was included as a random effect to account for technical variability and reduce batch effects associated with this factor.

Finally, given the limited sample size, a simulation-based sensitivity power analysis was performed in R using the **pwrEWAS** package. Simulations reflected the effective sample size after quality control, whole-blood DNA methylation data, the limma-based analytical approach, and a Benjamini-Hochberg FDR threshold of 0.05. Maximum target methylation differences (Δβ) of 0.05, 0.10, 0.15, and 0.20 were evaluated. Because power under FDR control depends on the assumed number of truly differentially methylated CpGs, sensitivity analyses were performed assuming 10, 100, or 1000 true differentially methylated CpGs. For each scenario, 50,000 CpG sites were simulated across 100 iterations.

3. Results

3.1. Quality control outcomes

The quality control procedure led to the exclusion of two samples that did not meet the predefined quality threshold. At the probe level, filtering resulted in the removal of a substantial number of probes across multiple categories. Specifically, 11,782 probes were excluded due to detection *P*-values >0.01, 4314 probes for low beadcount, and 3738 probes located in non-CpG regions. In addition, 31,945 probes overlapping known SNPs and 11,759 multi-hit probes were removed to ensure specificity of genomic mapping. A total of 24,518 probes located on sex chromosomes were excluded to prevent sex-related confounding effects. Furthermore, 50,209 probes flagged for reliability concerns, 7516 probes not properly mapped to the GRCh38/hg38 reference genome, and 6963 duplicate probes on the EPICv2 platform were discarded. Outlier detection using the MeCall.Outlier function did not identify any additional samples requiring exclusion, indicating overall homogeneity of the dataset after preprocessing. Importantly, the evaluation of potential batch effects using MeCall.FindBatch did not reveal significant technical variation, and therefore, no batch correction was applied. After completion of the entire preprocessing workflow, a total of 30 high-quality samples and a total of 816,007 unique CpG sites remained available for the subsequent analysis.

3.2. Peripheral immune composition in pathogenic vs non-pathogenic AFD variant carriers

Fig. 1 shows the distribution of estimated leukocyte proportions in carriers of pathogenic (ClinVar = 1) and non-pathogenic (ClinVar = 0) GLA variants. Formal statistical comparisons did not identify significant differences between groups for CD8+ T cells ($P = 0.478$), CD4+ T cells ($P = 0.947$), NK cells ($P = 0.550$), B cells ($P = 0.919$), monocytes ($P = 0.310$), or neutrophils ($P = 0.877$). All comparisons remained non-significant after Benjamini–Hochberg correction for multiple testing (FDR = 0.947 for all cell populations). Thus, although modest differences in the graphical distributions were observed for some leukocyte populations, there was no statistical evidence of systematic differences in estimated leukocyte composition between carriers of pathogenic and non-pathogenic GLA variants (Supplementary Table S1).

3.3. Epigenetic age acceleration in pathogenic vs non-pathogenic AFD variants

Epigenetic age acceleration (EAA) was compared between individuals carrying pathogenic AFD variants (ClinVar = 1) and those with non-pathogenic variants (ClinVar = 0) using multiple established epigenetic clocks (Horvath, Hannum, PhenoAge, Skin & Blood, and GrimAge) as well as the DunedinPACE estimator (Fig. 2).

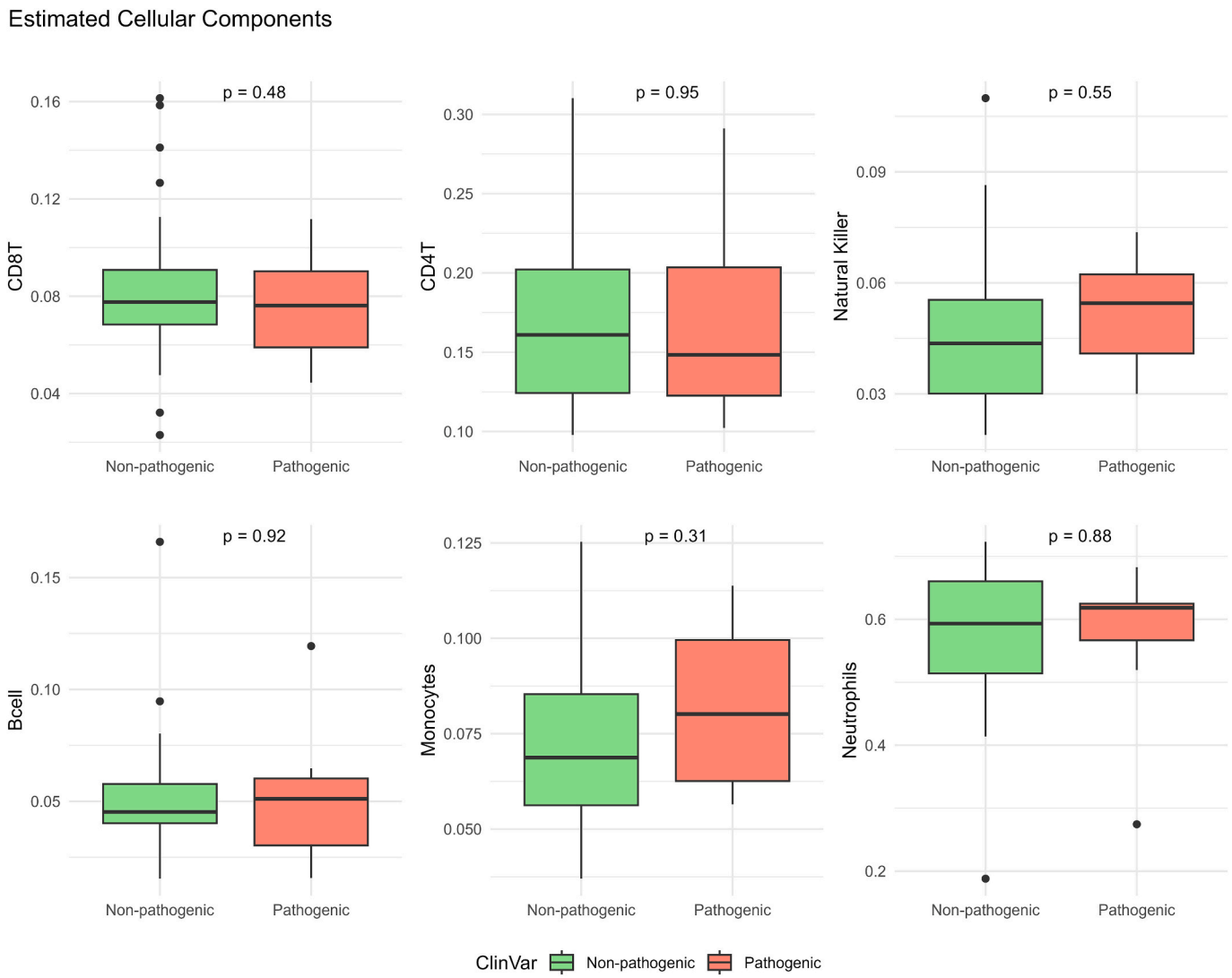

Fig. 1. Estimated leukocyte composition according to GLA variant classification. Boxplots show the estimated proportions of CD8+ T cells, CD4+ T cells, NK cells, B cells, monocytes, and neutrophils in carriers of non-pathogenic (ClinVar = 0, green; $n = 22$) and pathogenic (ClinVar = 1, red; $n = 8$) GLA variants. *P*-values shown in each panel were calculated using Welch's two-sample *t*-test. (For interpretation of the references to colour in this figure legend, the reader is referred to the web version of this article.)

No statistically significant differences were observed for the conventional epigenetic aging measures including Horvath (mean difference = 1.435, 95% CI: −7.804 to 10.675; $P = 0.741$), Hannum (mean difference = 2.951, 95% CI: −4.936 to 10.838; $P = 0.434$), PhenoAge (mean difference = 3.153, 95% CI: −9.544 to 15.849; $P = 0.596$), Skin & Blood (mean difference = 2.749, 95% CI: −5.924 to 11.422; $P = 0.503$), and GrimAge clocks (mean difference = 1.620, 95% CI: −0.843 to 4.082; $P = 0.187$). In contrast, DunedinPACE was significantly higher in carriers of pathogenic variants, with a mean between-group difference of 0.118 (95% CI: 0.011 to 0.224; $P = 0.0328$), indicating a faster estimated pace of biological aging in this group.

3.4. Identification of differentially methylated positions

A simulation-based sensitivity power analysis confirmed the limited power of the epigenome-wide CpG-based association analysis. In fact, across several scenarios assuming 10–1000 true DMPs, estimated power remained below 50% for all evaluated target methylation differences ($\Delta\beta = 0.05$–0.20).

As an exploratory epigenome-wide analysis, the comparison between carriers of pathogenic and non-pathogenic *GLA* variants identified 11 DMPs showing nominal evidence of methylation differences at a stringent nominal significance threshold ($p \leq 1 \times 10^{-5}$, Table 2).

Overall, the identified CpGs were almost evenly distributed in terms of directionality, with 6 loci showing reduced methylation and 5 displaying increased methylation in pathogenic carriers compared with non-pathogenic individuals. The differentially methylated sites were located across different chromosomes, and no evident clustering within a specific genomic region was observed (Fig. 3). This distribution suggests that the methylation differences are dispersed throughout the genome rather than concentrated within a single differentially methylated region.

The volcano plot (Fig. 4) illustrated a balanced pattern of hyper- and hypomethylation among the top-ranking CpGs, without evidence of a generalized shift toward either global hypermethylation or hypomethylation. Instead, the data indicate a bidirectional remodeling of methylation at selected loci.

To further explore these differences at the sample level, boxplots of M-values were generated for the most significant CpGs (Fig. 5).

These visualizations confirmed the direction of effect identified by the regression analysis. In several loci, pathogenic carriers showed a clear shift in median methylation compared with non-pathogenic

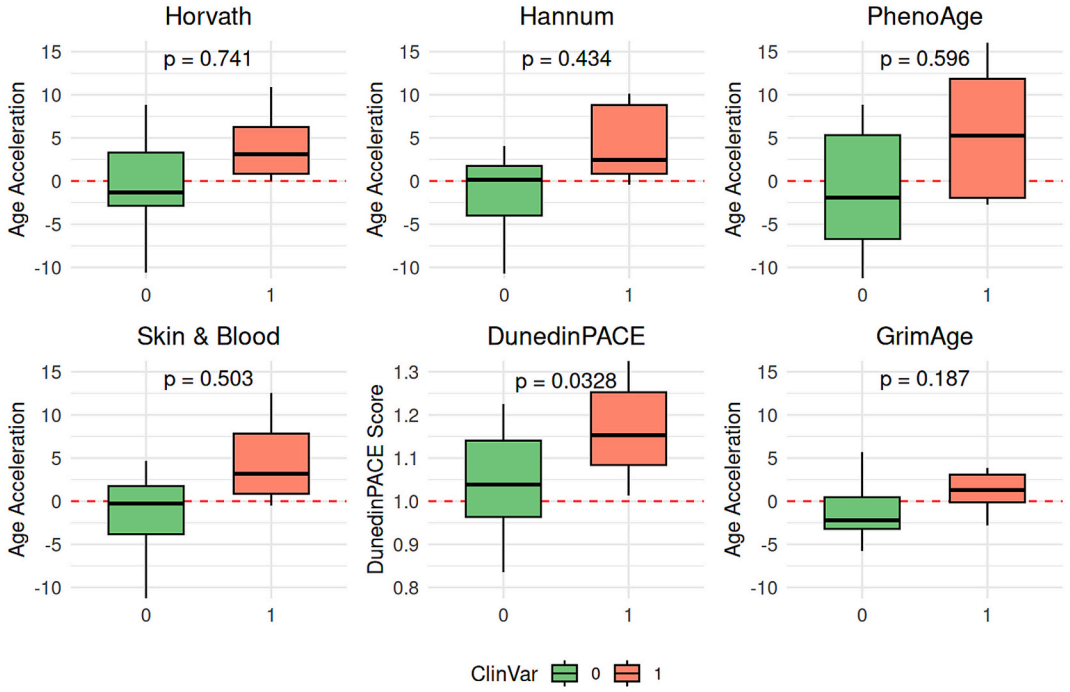

Fig. 2. Distribution of epigenetic age acceleration across ClinVar groups. Boxplots show epigenetic age acceleration according to the Horvath, Hannum, PhenoAge, Skin & Blood, DunedinPACE and GrimAge measures in carriers of non-pathogenic (ClinVar = 0; $n = 22$) and pathogenic (ClinVar = 1; $n = 8$) GLA variants.

Table 2
Top-ranking differentially methylated CpG loci between carriers of pathogenic and non-pathogenic GLA variants. Effect estimates (logFC) and corresponding 95% confidence intervals (CI) are reported to provide information on the magnitude and precision of the observed methylation differences.

CpG	Chromosome	Position	Gene	logFC (95% CI)	*P*-value	FDR
cg18020065	chr13	114064258	*RASA3*	1.023 (0.701 to 1.345)	9.58×10^{-7}	5.32×10^{-1}
cg00783409	chr8	1841122	*ARHGEF10*	−1.220 (−1.624 to −0.815)	2.10×10^{-6}	5.32×10^{-1}
cg22334000	chr4	80335845	*CFAP299*	−0.826 (−1.102 to −0.550)	2.34×10^{-6}	5.32×10^{-1}
cg25935178	chr1	159900112	*CFAP45*	0.744 (0.489 to 0.999)	3.46×10^{-6}	5.32×10^{-1}
cg02472935	chr15	52419622	*MYO5A*	−0.953 (−1.285 to −0.621)	4.28×10^{-6}	5.32×10^{-1}
cg16711522	chr15	52466080	*MYO5A*	0.986 (0.640 to 1.332)	4.85×10^{-6}	5.32×10^{-1}
cg04977659	chr20	63756641	*ZBTB46*	−1.366 (−1.847 to −0.885)	5.05×10^{-6}	5.32×10^{-1}
cg22138327	chr13	27425040	*GTF3A*	1.728 (1.118 to 2.337)	5.22×10^{-6}	5.32×10^{-1}
cg06136473	chr19	41546287	–	0.738 (0.472 to 1.005)	7.19×10^{-6}	5.32×10^{-1}
cg11564495	chr1	115842508	*NHLH2*	−0.758 (−1.031 to −0.484)	7.33×10^{-6}	5.32×10^{-1}
cg13615077	chr1	6320962	*ACOT7*	−0.611 (−0.836 to −0.386)	9.81×10^{-6}	6.90×10^{-1}

individuals, although partial overlap between groups was present. Despite the limited sample size and inter-individual variability, the separation observed in the boxplots was consistent with the corresponding logFC estimates derived from the linear model.

The most strongly associated CpGs included *cg18020065* on chromosome 13, annotated to *RASA3*, which was hypomethylated in pathogenic carriers (logFC = +1.02), and *cg00783409* on chromosome 8, annotated to *ARHGEF10*, which showed higher methylation in pathogenic carriers (logFC = −1.22). Additional loci were annotated to *CFAP299* (*cg22334000*, chr4), *CFAP45* (*cg25935178*, chr1), and two CpGs within *MYO5A* (*cg02472935* and *cg16711522*, chr15), displaying opposite directions of methylation change. Other associated genes included *ZBTB46* (chr20), *GTF3A* (chr13), *NHLH2* (chr1), and *ACOT7* (chr1).

From a genomic annotation perspective, several CpGs were located within regulatory contexts, including CpG islands, shores, shelves, and promoter-associated regions. This positional distribution is compatible with a potential involvement in transcriptional regulation, although functional consequences cannot be inferred directly from methylation levels alone.

However, none of these CpG loci remained statistically significant after correction for multiple testing (all FDR > 0.05). Consequently, these findings should be considered exploratory and hypothesis-generating.

4. Discussion

In this study, we investigated genome-wide DNA methylation differences between pathogenic and non-pathogenic AFD carriers and explored epigenetic age acceleration as a potential modifier of phenotypic variability. Although no loci remained significant after correction for multiple testing, this exploratory methylome-wide analysis identified a subset of CpG sites displaying coherent methylation differences between pathogenic and non-pathogenic carriers, supporting the presence of preliminary epigenetic signatures potentially associated with disease-related biological processes. Importantly, the identified CpGs were distributed across multiple chromosomes and did not cluster within a specific genomic region, indicating that epigenetic variation in AFD may involve dispersed regulatory mechanisms rather than a single differentially methylated region. The balanced pattern of hyper- and hypomethylation observed in the volcano plot further supports the idea of locus-specific remodeling rather than global methylation shifts.

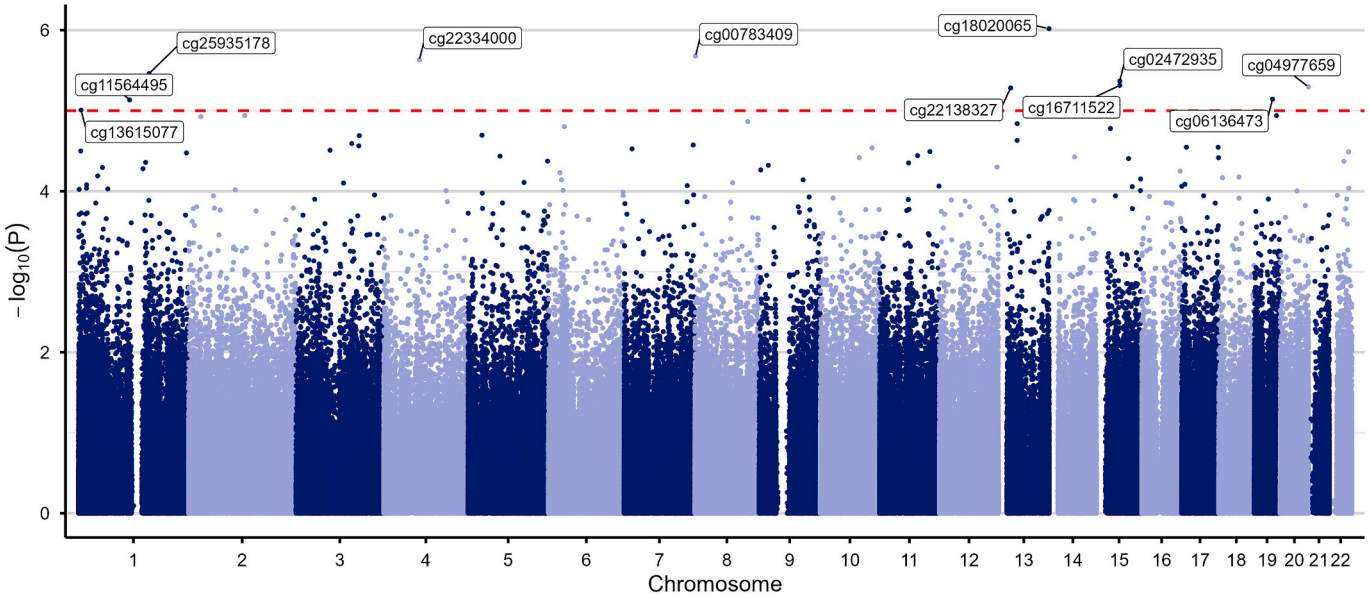

Fig. 3. Manhattan plot of the exploratory epigenome-wide differential methylation analysis comparing carriers of non-pathogenic (ClinVar = 0; $n = 22$) and pathogenic (ClinVar = 1; $n = 8$) GLA variants. The horizontal red dashed line indicates the nominal significance threshold of $P = 1 \times 10^{-5}$ [−log10(P) = 5]. (For interpretation of the references to colour in this figure legend, the reader is referred to the web version of this article.)

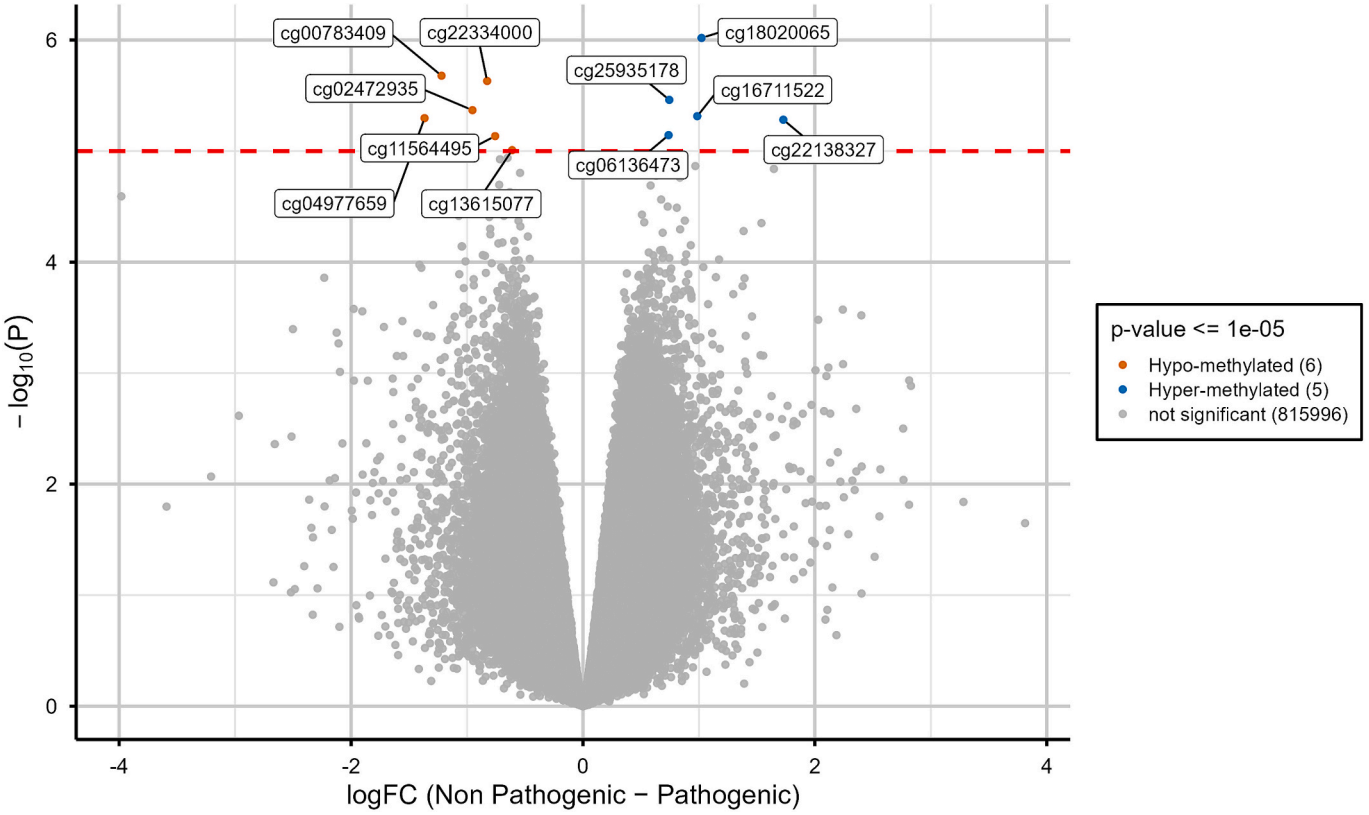

Fig. 4. Volcano plot of the exploratory epigenome-wide differential methylation analysis comparing carriers of non-pathogenic (ClinVar = 0; $n = 22$) and pathogenic (ClinVar = 1; $n = 8$) GLA variants. The horizontal red dashed line indicates the nominal significance threshold of $P = 1 \times 10^{-5}$ [−log10(P) = 5]. (For interpretation of the references to colour in this figure legend, the reader is referred to the web version of this article.)

Several of the annotated genes are involved in biological pathways plausibly related to AFD pathophysiology. The most significant locus, *cg18020065*, mapped to *RASA3*, a Ras GTPase-activating protein that negatively regulates Ras signaling and is essential for vascular and hematopoietic integrity (Molina-Ortiz et al., 2018). *RASA3* has been shown to play a role in platelet production and endothelial homeostasis. Given that AFD is characterized by endothelial dysfunction, microvascular injury, and pro-thrombotic alterations secondary to globotriaosylceramide accumulation (Spero and Roisen, 1985), differential methylation at *RASA3* may reflect altered vascular signaling pathways in pathogenic

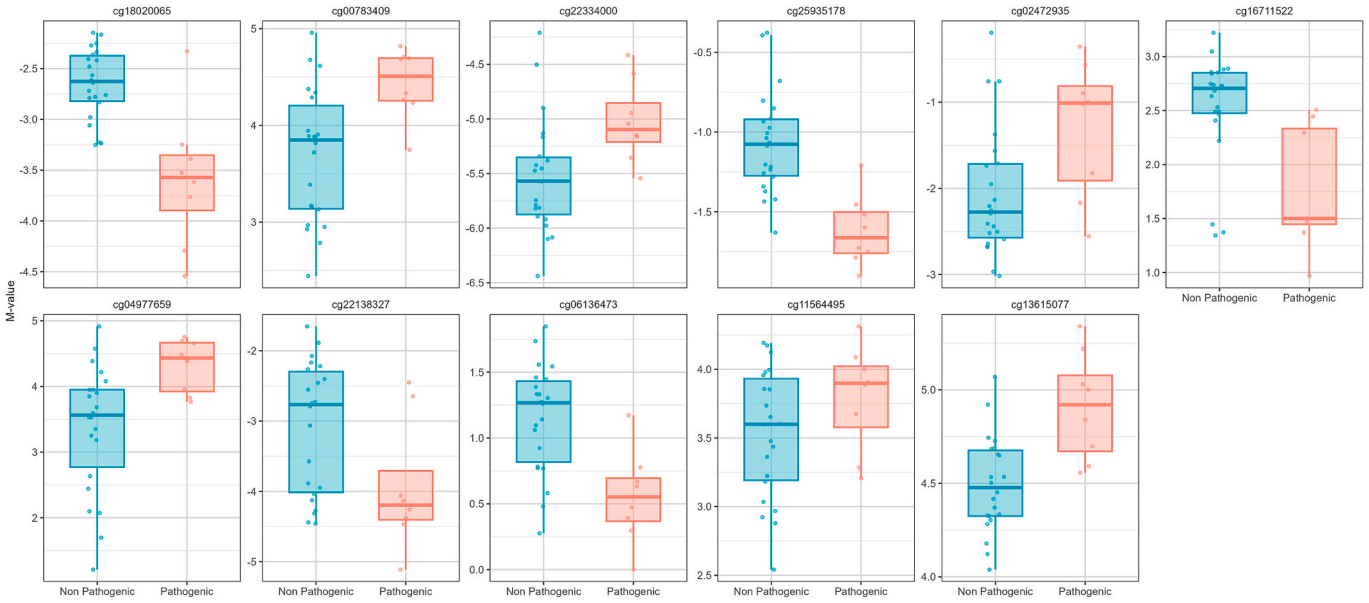

Fig. 5. Boxplots showing M-value distributions for the top-ranking CpG loci identified in the exploratory differential methylation analysis in carriers of non-pathogenic (ClinVar = 0; $n = 22$) and pathogenic (ClinVar = 1; $n = 8$) GLA variants.

carriers. However, the biological interpretation of the observed hypomethylation at *cg18020065* requires caution, as this CpG is located within the gene body rather than in a canonical promoter region, where the relationship between DNA methylation and transcriptional output is not necessarily inverse. Indeed, intragenic methylation may show context-dependent positive or negative correlations with gene expression. Therefore, while our findings raise the hypothesis that *RASA3*-mediated signaling may act as an epigenetic modifier of vascular phenotype in AFD disease, the current methylation data alone do not allow direct inference of *RASA3* overexpression, and further transcriptomic and protein-level validation studies are warranted. *Cg00783409* was annotated to *ARHGEF10*, a Rho guanine nucleotide exchange factor involved in cytoskeletal organization and peripheral nerve function (Lu et al., 2017). *ARHGEF10* mutations have been associated with slowed nerve conduction and altered myelination. Considering that neuropathic pain and small fiber neuropathy are hallmark manifestations of AFD (Biegstraaten et al., 2013), epigenetic modulation of genes regulating axonal structure and cytoskeletal dynamics may contribute to inter-individual variability in neurological involvement. Two CpGs mapped to *MYO5A*, encoding myosin Va, an actin-based motor protein involved in vesicular trafficking and organelle transport (Van Gele et al., 2009). *MYO5A* is critical for intracellular cargo transport and lysosome positioning. Since AFD is a lysosomal storage disorder characterized by impaired glycosphingolipid degradation and lysosomal dysfunction (Phadke et al., 2009), methylation changes in genes regulating vesicular trafficking may represent adaptive or compensatory responses to altered intracellular transport dynamics. Methylation differences were also observed in *CFAP45* and *CFAP299*, genes implicated in ciliary and flagellar function. While not directly linked to AFD, primary cilia are increasingly recognized as regulators of endothelial signaling and vascular homeostasis (Dougherty et al., 2020). Given the central role of vascular dysfunction in AFD, dysregulation of cilia-associated genes may indirectly influence endothelial responses to metabolic stress. *Cg04977659* mapped to *ZBTB46*, a transcription factor selectively expressed in classical dendritic cells and endothelial cells, where it regulates immune activation (Kabir et al., 2024). Chronic inflammation is a recognized component of AFD pathophysiology, with elevated pro-inflammatory cytokines reported in affected individuals (Coelho-Ribeiro et al., 2024). Epigenetic modulation of immune-related transcription factors may therefore contribute to variability in systemic inflammatory responses among carriers. Similarly, *ACOT7*, identified at *cg13615077*, encodes acyl-CoA thioesterase 7, an enzyme involved in lipid metabolism and fatty acid turnover (Kumar et al., 2023). AFD is characterized by glycosphingolipid accumulation and broader alterations in lipid handling (Germain et al., 2022), suggesting that methylation changes in lipid metabolism genes may reflect metabolic stress pathways secondary to lysosomal dysfunction. *NHLH2*, associated with *cg11564495*, encodes a basic helix-loop-helix transcription factor involved in neuroendocrine and energy balance regulation (Fox et al., 2007). Although not previously linked to AFD, dysregulation of energy metabolism and systemic stress pathways may influence disease progression and organ involvement.

Overall, many of the identified genes converge on biological domains consistent with established mechanisms in AFD, including vascular signaling, cytoskeletal organization, intracellular trafficking, lipid metabolism, and immune regulation. While preliminary and hypothesis-generating, these findings support the possibility that autosomal DNA methylation remodeling may contribute to inter-individual variability in AFD by modulating pathways involved in vascular homeostasis, immune activation, intracellular trafficking, and metabolic stress responses. These functional annotations provide a biological context for the exploratory methylation signals but should not be interpreted as evidence that these genes are functionally altered in AFD. In particular, DNA methylation changes do not necessarily translate into altered gene expression, and their effects depend on genomic location and regulatory context. Moreover, no transcriptomic, protein-expression, or functional analyses were performed in the present study. Therefore, these loci should be regarded exclusively as hypothesis-generating candidates whose potential relevance to AFD requires independent replication and functional validation.

With respect to epigenetic aging, our analysis revealed a consistent trend toward increased biological age acceleration in carriers of pathogenic AFD variants compared with non-pathogenic individuals. Across multiple established clocks, pathogenic carriers exhibited higher median age acceleration values, with the most evident separation observed for the Hannum and PhenoAge estimators. Importantly, DunedinPACE values were also higher in the pathogenic group, indicating an increased pace of biological aging rather than solely cumulative age deviation. However, no statistically significant differences were observed between carriers of pathogenic and non-pathogenic GLA variants for the Horvath,

Hannum, PhenoAge, Skin & Blood, or GrimAge age-acceleration measures. Although some clocks showed descriptive differences in median values, these findings should not be interpreted as evidence of accelerated epigenetic aging. In contrast, DunedinPACE was significantly higher in carriers of pathogenic variants, suggesting a faster estimated pace of biological aging in this group. This distinction is biologically relevant because DunedinPACE differs conceptually from conventional epigenetic clocks. Whereas conventional clocks primarily quantify differences between DNA methylation-predicted age and chronological age, DunedinPACE was specifically developed to estimate the pace at which biological aging is occurring. Thus, the present findings do not indicate that carriers of pathogenic variants are consistently epigenetically older according to multiple clocks; rather, they provide preliminary evidence that these individuals may exhibit a faster pace of biological aging. Given the limited sample size and the nominal significance of this finding, however, replication in larger independent cohorts is required. Importantly, this acceleration pattern can be interpreted in light of the locus-specific methylation changes observed in the differential analysis. Chronic glycosphingolipid accumulation in AFD is associated with sustained metabolic, inflammatory, and vascular stress, biological processes that may influence both DNA methylation patterns and aging-related molecular signatures. In this framework, locus-specific methylation differences and epigenetic aging measures may provide complementary, although distinct, information on disease-related biological processes. However, given the exploratory nature of the methylation findings and the absence of functional validation, a direct mechanistic relationship between these observations cannot be established.

Several limitations must be acknowledged. The sample size was limited, with 30 participants included after quality control (22 non-pathogenic and 8 pathogenic variant carriers). Given the small and unbalanced groups and the large number of CpG sites tested genome-wide, statistical power to detect small-to-moderate methylation differences after correction for multiple testing was limited. This likely contributed to the absence of FDR-significant loci and limits the reliability and generalizability of individual CpG associations. Accordingly, the nominally associated loci identified in this study should be interpreted exclusively as exploratory, hypothesis-generating candidates requiring replication in larger independent cohorts. Conversely, the absence of FDR-significant associations should not be interpreted as evidence for the absence of methylation differences, given the limited statistical power of the present analysis. In addition, DNA methylation was assessed in peripheral blood, which may not fully capture tissue-specific alterations in kidney, heart, or nervous system, the primary organs affected in FD. The cross-sectional design precludes causal inference regarding whether methylation differences are drivers or consequences of disease progression. An additional limitation concerns the composition of the comparison groups. The non-pathogenic group included several individuals carrying GLA variants classified as VUS and therefore cannot be considered equivalent to a healthy or unaffected control population. Consequently, the present comparison should be interpreted as an exploratory within-cohort analysis according to GLA variant classification, rather than as a case-control comparison. Furthermore, the nominally associated CpG loci identified in this exploratory analysis were not validated using an independent cohort or an orthogonal methylation assay. Given that none of these loci survived correction for multiple testing, they should be regarded as hypothesis-generating candidates rather than validated methylation biomarkers. Replication in larger independent cohorts, followed by targeted validation using approaches such as pyrosequencing or bisulfite sequencing, will be necessary to establish their robustness. Finally, an additional limitation is the absence of a healthy control group. Consequently, the methylation differences observed between carriers of pathogenic and non-pathogenic GLA variants cannot be interpreted as AFD-specific epigenetic alterations, nor can we exclude that some of these differences reflect normal inter-individual epigenetic variability. The present findings should therefore be interpreted exclusively as within-cohort exploratory associations with GLA variant classification. Future studies including age- and sex-matched healthy controls will be required to determine whether these methylation patterns are specifically associated with AFD. Despite these limitations, this study represents the first genome-wide exploration of autosomal DNA methylation signatures in AFD carriers beyond X-chromosome inactivation mechanisms. While preliminary, the identified loci highlight biologically plausible pathways that warrant validation in larger, independent cohorts and functional studies.

5. Conclusions

Taken together, this exploratory study identified nominal autosomal DNA methylation differences between carriers of pathogenic and non-pathogenic GLA variants, none of which remained significant after correction for multiple testing. Among the biological aging measures examined, only DunedinPACE differed significantly between groups, with higher values observed in carriers of pathogenic variants. These preliminary findings raise the possibility that the pace of biological aging may differ according to GLA variant classification, but require confirmation in larger, independent cohorts including healthy controls. Future studies integrating DNA methylation with transcriptomic data will be particularly important to determine whether reproducible methylation differences are associated with altered gene expression. Integration with proteomic and functional data, together with detailed clinical phenotyping, will ultimately be required to establish the biological relevance of candidate epigenetic loci in AFD.

CRediT authorship contribution statement

Mirella Aurora Aceto: Methodology, Formal analysis, Data curation. **Ersilia Paparazzo:** Methodology, Formal analysis, Data curation. **Gemma Antonucci:** Methodology, Data curation. **Rosita Greco:** Methodology, Data curation. **Michele Andreucci:** Writing – review & editing, Investigation. **Teresa Serra Cassano:** Methodology, Data curation. **Pierluigi Mercatante:** Methodology, Data curation. **Giuseppe Passarino:** Writing – review & editing, Investigation, Funding acquisition. **Antonella La Russa:** Methodology, Data curation. **Alberto Montesanto:** Writing – original draft, Supervision, Methodology, Conceptualization.

Ethical approval

This study was approved by the Regional Ethical Committee, Catanzaro, Italy (Prot. CET 200/2024).

Funding

This work was supported by the Next Generation EU, in the context of the National Recovery and Resilience Plan, with the Project PE8 – Project Age-It: "Ageing Well in an Ageing Society" financed by the Next Generation EU [DM 1557 11.10.2022].

Declaration of competing interest

The authors declare that they have no known competing financial interests or personal relationships that could have appeared to influence the work reported in this paper.

Acknowledgement

We acknowledge co-funding from Next Generation EU, in the context of the National Recovery and Resilience Plan, with the Project PE8 – Project Age-It: "Ageing Well in an Ageing Society" [DM 1557 11.10.2022].

Appendix A. Supplementary data

Supplementary data to this article can be found online at https://doi.org/10.1016/j.exger.2026.113318.

Data availability

Data will be made available on request.

References

Aryee, M.J., et al., 2014. Minfi: a flexible and comprehensive bioconductor package for the analysis of Infinium DNA methylation microarrays. Bioinforma. Oxf. Engl. 30, 1363–1369.

Balaton, B.P., Dixon-McDougall, T., Peeters, S.B., Brown, C.J., 2018. The eXceptional nature of the X chromosome. Hum. Mol. Genet. 27, R242–R249.

Belsky, D.W., et al., 2022. DunedinPACE, a DNA methylation biomarker of the pace of aging. eLife 11, e73420.

Biegstraaten, M., Linthorst, G.E., van Schaik, I.N., Hollak, C.E.M., 2013. Fabry disease: a rare cause of neuropathic pain. Curr. Pain Headache Rep. 17, 365.

Coelho-Ribeiro, B., et al., 2024. Inflammation and exosomes in Fabry disease pathogenesis. Cells 13, 654.

De Riso, G., et al., 2020. Ultra-deep DNA methylation analysis of X-linked genes: GLA and AR as model genes. Genes 11, 620.

Di Risi, T., et al., 2021. DNA methylation impact on Fabry disease. Clin. Epigenetics 13, 24.

Di Risi, T., et al., 2022. Methylome profiling in Fabry disease in clinical practice: a proof of concept. Int. J. Mol. Sci. 23, 12110.

Dougherty, G.W., et al., 2020. CFAP45 deficiency causes situs abnormalities and asthenospermia by disrupting an axonemal adenine nucleotide homeostasis module. Nat. Commun. 11, 5520.

Du, P., et al., 2010. Comparison of Beta-value and M-value methods for quantifying methylation levels by microarray analysis. BMC Bioinform. 11, 587.

Fox, D.L., Vella, K.R., Good, D.J., 2007. Energy balance pathways converging on the Nhlh2 transcription factor. Front. Biosci. J. Virtual Libr. 12, 3983–3993.

Freire-Aradas, A., et al., 2020. A comparison of forensic age prediction models using data from four DNA methylation technologies. Front. Genet. 11, 932.

Furlan, G., Galupa, R., 2023. Correction: Furlan, G. and Galupa R. Mechanisms of choice in X-chromosome inactivation. Cells 2022, 11, 535. Cells 12, 950.

Garali, I., et al., 2020. Improvements and inter-laboratory implementation and optimization of blood-based single-locus age prediction models using DNA methylation of the ELOVL2 promoter. Sci. Rep. 10, 15652.

Germain, D.P., et al., 2022. An expert consensus on practical clinical recommendations and guidance for patients with classic Fabry disease. Mol. Genet. Metab. 137, 49–61.

Hannum, G., et al., 2013. Genome-wide methylation profiles reveal quantitative views of human aging rates. Mol. Cell 49, 359–367.

Horvath, S., 2013. DNA methylation age of human tissues and cell types. Genome Biol. 14, R115.

Horvath, S., et al., 2018. Epigenetic clock for skin and blood cells applied to Hutchinson Gilford Progeria Syndrome and ex vivo studies. Aging 10, 1758–1775.

Houseman, E.A., et al., 2012. DNA methylation arrays as surrogate measures of cell mixture distribution. BMC Bioinform. 13, 86.

Iza, S.N., Lagos, S.Y.O., Yunis, J.J., 2025. DNA methylation analysis and phenotype severity in Fabry disease. J. Inborn Errors Metab. Screen. 13, e20230007.

Kabir, A.U., et al., 2024. ZBTB46 coordinates angiogenesis and immunity to control tumor outcome. Nat. Immunol. 25, 1546–1554.

Kumar, M., et al., 2023. Amyloid fibril formation, structure and domain swapping of acyl-coenzyme A thioesterase-7. FEBS J. 290, 4057–4073.

Levine, M.E., et al., 2018. An epigenetic biomarker of aging for lifespan and healthspan. Aging 10, 573–591.

Lu, D.-H., et al., 2017. ARHGEF10 knockout inhibits platelet aggregation and protects mice from thrombus formation. J. Thromb. Haemost. JTH 15, 2053–2064.

Molina-Ortiz, P., et al., 2018. Rasa3 controls turnover of endothelial cell adhesion and vascular lumen integrity by a Rap1-dependent mechanism. PLoS Genet. 14, e1007195.

Pelegí-Sisó, D., de Prado, P., Ronkainen, J., Bustamante, M., González, J.R., 2021. methylclock: a Bioconductor package to estimate DNA methylation age. Bioinformatics 37, 1759–1760.

Peters, T.J., et al., 2015. De novo identification of differentially methylated regions in the human genome. Epigenetics Chromatin 8, 6.

Phadke, S.R., Mandal, K., Girisha, K.M., 2009. Fabry disease: a treatable lysosomal storage disorder. Natl Med. J. India 22, 20–22.

Pieroni, M., Namdar, M., Olivotto, I., Desnick, R.J., 2024. Anderson–Fabry disease management: role of the cardiologist. Eur. Heart J. 45, 1395–1409.

Řeboun, M., et al., 2022. Pitfalls of X-chromosome inactivation testing in females with Fabry disease. Am. J. Med. Genet. A 188, 1979–1989.

Robinson, G.K., 1991. That BLUP is a Good thing: the estimation of random effects. Stat. Sci. 6.

Schiffmann, R., 2024. Investigating Fabry disease - some lessons learned. Rare Dis. Orphan Drugs J. 3.

Simonetta, I., et al., 2018. Genetics and gene therapy of Anderson-Fabry disease. Curr. Gene Ther. 18, 96–106.

Spero, D.A., Roisen, F.J., 1985. Neuro-2a neuroblastoma cells form neurites in the presence of taxol and cytochalasin D. Brain Res. 355, 155–159.

Teschendorff, A.E., Horvath, S., 2025. Epigenetic ageing clocks: statistical methods and emerging computational challenges. Nat. Rev. Genet. 26, 350–368.

Tuttolomondo, A., et al., 2013. Anderson-Fabry disease: a multiorgan disease. Curr. Pharm. Des. 19, 5974–5996.

Tuttolomondo, A., et al., 2017. Inter-familial and intra-familial phenotypic variability in three Sicilian families with Anderson-Fabry disease. Oncotarget 8, 61415–61424.

Van Gele, M., Dynoodt, P., Lambert, J., 2009. Griscelli syndrome: a model system to study vesicular trafficking. Pigm. Cell Melanoma Res. 22, 268–282.

Viggiano, E., Politano, L., 2021. X chromosome inactivation in carriers of Fabry disease: review and meta-analysis. Int. J. Mol. Sci. 22, 7663.

Wagenhäuser, L., et al., 2022. X-chromosomal inactivation patterns in women with Fabry disease. Mol. Genet. Genomic Med. 10, e2029.

Yang, H.-H., Han, M.-R., 2024. MethylCallR: a comprehensive analysis framework for Illumina Methylation Beadchip. Sci. Rep. 14, 27026.

Zarate, Y.A., Hopkin, R.J., 2008. Fabry's disease. Lancet 372, 1427–1435.

Zou, H., Hastie, T., 2005. Regularization and variable selection via the elastic net. J. R. Stat. Soc. Ser. B Stat Methodol. 67, 301–320.